

Microcanonical unimolecular rate theory at surfaces. III. Thermal dissociative chemisorption of methane on Pt(111) and detailed balance

A. Bukoski, H. L. Abbott, and I. Harrison^{a)}

Department of Chemistry, University of Virginia, Charlottesville, Virginia 22904-4319

(Received 11 March 2005; accepted 29 June 2005; published online 7 September 2005)

A local hot spot model of gas-surface reactivity is used to investigate the state-resolved dynamics of methane dissociative chemisorption on Pt(111) under thermal equilibrium conditions. Three Pt surface oscillators, and the molecular vibrations, rotations, and the translational energy directed along the surface normal are treated as active degrees of freedom in the 16-dimensional microcanonical kinetics. Several energy transfer models for coupling a local hot spot to the surrounding substrate are developed and evaluated within the context of a master equation kinetics approach. Bounds on the thermal dissociative sticking coefficient based on limiting energy transfer models are derived. The three-parameter physisorbed complex microcanonical unimolecular rate theory (PC-MURT) is shown to closely approximate the thermal sticking under any realistic energy transfer model. Assuming an apparent threshold energy for CH₄ dissociative chemisorption of $E_0=0.61$ eV on clean Pt(111), the PC-MURT is used to predict angle-resolved yield, translational, vibrational, and rotational distributions for the reactive methane flux at thermal equilibrium at 500 K. By detailed balance, these same distributions should be observed for the methane product from methyl radical hydrogenation at 500 K in the zero coverage limit if the methyl radicals are not subject to side reactions. Given that methyl radical hydrogenation can only be experimentally observed when the CH₃ radicals are kinetically stabilized against decomposition by coadsorbed H, the PC-MURT was used to evaluate E_0 in the high coverage limit. A high coverage value of $E_0=2.3$ eV adequately reproduced the experimentally observed methane angular and translational energy distributions from thermal hydrogenation of methyl radicals. Although rigorous application of detailed balance arguments to this reactive system cannot be made because thermal decomposition of the methyl radicals competes with hydrogenation, approximate applicability of detailed balance would argue for a strong coverage dependence of E_0 with H coverage—a dependence not seen for methyl radical hydrogenation on Ru(0001), but not yet experimentally explored on Pt(111). © 2005 American Institute of Physics. [DOI: 10.1063/1.2006679]

I. INTRODUCTION

Understanding the dynamics and mechanism of the activated dissociative chemisorption of molecules on surfaces is a central goal of surface science. Interest in this class of surface reactions is being driven by their importance as key steps in many industrial catalytic¹ and chemical-vapor deposition² processes, their utility as model systems for the study of gas-surface interactions,³ and the availability of energy- and state-selected dissociative sticking coefficient data from new supersonic molecular beam techniques that can initiate reactions on different portions of the reactive potential energy surface.⁴ Progress towards uniting experimental studies of ultrahigh vacuum surface science on single crystal surfaces with high pressure catalysis has been hampered because surface science experiments are often performed under nonequilibrium conditions that bear little resemblance to the thermal equilibrium conditions of industrial catalysis at some 15 orders of magnitude higher pressure. Important efforts to bridge this “pressure gap” have involved intermediate pressure (ca. millibar) bulb

experiments⁵ performed under thermal equilibrium conditions that can provide the thermal activation energy and sticking probabilities that better approximate those appropriate to the high pressure environment of modern catalysis. However, as with molecular beam surface science experiments, thermal bulb experiments are notoriously difficult to perform.

Based on a large body of experimental data and theoretical investigations the dissociation of methane on various transition metal surfaces such as Ni,^{4–15} Pd,¹⁶ Pt,^{17–24} Ir,^{25–27} Ru,^{28,29} and W^{30,31} has emerged as the polyatomic model system for activated dissociative chemisorption. In an earlier paper on the dissociation of methane on Pt(111),²² a microcanonical unimolecular rate theory (MURT) for activated dissociative chemisorption was described. A master equation (ME) was used to explicitly account for the effects of vibrational energy transfer to the surface during the reactive collision. A truncated version of the ME-MURT that neglects energy transfer to the surface subsequent to the initial gas-surface impact and assumes that energy is randomized in the transient gas-surface collision complex formed in the vicinity of the physisorption well was described as the physisorbed complex (PC)-MURT. The PC-MURT provides a consistent

^{a)}Fax: (434) 924-3710; electronic mail: harrison@virginia.edu

analysis and prediction framework for nonequilibrium experiments, recovers canonical transition state theory and Arrhenius sticking coefficients for thermal equilibrium experiments, makes contact with electronic structure theory by the definition of transition state characteristics, and is not very computationally demanding. The PC-MURT also provides a statistical base line for gas-surface reactivity against which dynamical behavior, such as mode-specific chemistry, can be identified when it occurs.^{12,14,15} A three-parameter PC-MURT model was used to simulate supersonic molecular beam measurements of methane dissociative sticking coefficients on Pt(111) as functions of molecular translational and vibrational energies, isotope, and surface temperature.²² The simulations indicate that the apparent threshold energy for CH₄ dissociative chemisorption on clean Pt(111) is $E_0=0.61$ eV.

The PC-MURT has also been used to predict the experimental thermal equilibrium, nonequilibrium, and eigenstate-resolved dissociative sticking coefficients for methane on Ni(100) over roughly ten orders of magnitude variation in both pressure and sticking.^{32,33,14} The apparent threshold energy for CH₄ dissociation on Ni(100) is $E_0=0.67$ eV, in agreement with the *ab initio* quantum chemistry prediction³⁴ of 0.69 ± 0.04 eV, and down from 4.48 eV in the gas phase. The diverse range of experimental studies and electronic structure calculations available for the CH₄/Ni(100) system make it an excellent proving ground for models of gas-surface reactivity involving polyatomic molecules. The vibrational state-resolved dissociative chemisorption of methane on Ni(100) was recently explored using the PC-MURT.¹⁴ Although the statistical PC-MURT model of surface reaction kinetics has enjoyed considerable quantitative success in linking disparate methane^{14,22,27} and silane³⁵ dissociative chemisorption experiments to one another and to the predictions of electronic structure theory, there are recent dynamical experiments that indicate, in some instances, there are mode-specific preferences for reaction from particular molecular states.^{12,15}

An alternative approach towards the study of activated dissociative chemisorption is to explore the dynamics of the reverse reaction, associative desorption, using the principle of detailed balance to relate the forward and reverse processes at thermal equilibrium. Associative desorption experiments can be used to derive sticking probabilities with full quantum state and translational energy resolution, providing a way to determine how internal energy influences dissociative chemisorption probabilities.³⁶ To date, the dissociation of diatomic hydrogen on Cu single-crystal surfaces stands as the most complete example of this type of investigation and serves as a prototype for activated dissociative chemisorption in general. Both direct sticking and associative desorption measurements have provided a consistent picture of the influence of translational and vibrational energies on H₂ dissociation. However, H₂ associative desorption experiments are complicated by the permeation route of supplying reactants to the surface and coverage-dependent effects which can alter the energetics of reaction. For dissociative chemisorption with polyatomic chemisorbed product species that can themselves decompose, the problem of side reactions must be

addressed. Reactant decomposition can channel reactive flux away from the assumed associative desorption/sticking equilibrium, thereby degrading the applicability of detailed balance.

Ukrainsev and Harrison³⁷ were the first to study the dissociative chemisorption of methane on Pt(111) via the application of detailed balance arguments.³⁸ Methane from methyl radical hydrogenation at 240 K displayed a strongly peaked around the surface normal, $\cos^{37} \vartheta$, angular distribution in the angle-resolved thermal programmed reaction, suggesting that dissociative chemisorption of methane on extensively H- and CH₃-covered Pt(111) surfaces should also display a sharply angle-dependent sticking coefficient. Given that molecular beam studies^{18,19} report that the initial dissociative sticking coefficient of methane on clean Pt(111) scales with the normal component of translational energy, $E_n=E_t \cos^2 \vartheta$, as $S(E_n)=0.073E_n^{4.27}$, one might anticipate that the desorption angular flux distribution should vary roughly as $\cos^{9.54} \vartheta$ by detailed balance. Watanabe *et al.*³⁹ used laser-induced thermal reaction to study the molecular and associative desorption of CD₄ from Pt(111). At 395 K surface temperature they found that the associative desorption angular dependence fitted a $\cos^{31} \vartheta$ distribution and found no dependence of the mean translational energy on the desorption angle from 0° to 25° from the surface normal. Applying the statistical model of Ukrainsev and Harrison³⁸ to their translational energy distribution along the surface normal Watanabe *et al.* concluded that a statistical description was insufficient to account for their observations. Watanabe *et al.* further concluded that statistical theories are incapable of predicting the partitioning of the available energy beyond the transition state when a large exit channel barrier is present. The latter conclusion is overestimated, because if detailed balance holds at the surface, then successful predictions by a statistical theory of the state-resolved dissociative sticking of CH₄, involving passage over a large entrance channel barrier, must uniquely fix the CH₄ product state distribution from CH₃ radical hydrogenation. Furthermore, detailed balance is rigorously applicable only under identical adsorption/desorption conditions. Desorption predictions based on initial dissociative sticking coefficients will apply only to recombinative desorption experiments in the zero coverage limit. Arguing along Evans-Polanyi lines that as the surface coverage increases the CH₄ dissociation products are destabilized, and so too is the reactive transition state, Harrison⁴⁰ found that the statistical model (an earlier approximate form of the PC-MURT) could account for most of the observations of Watanabe *et al.* If a coverage dependent barrier height to dissociative chemisorption was assumed, increasing the threshold energy for dissociation from a zero coverage value of 0.64 eV to a high coverage value of 1.2 eV recovered an agreement between the statistical theory and the CH₄ angular distribution and translational energy distribution along the surface normal of Watanabe *et al.*

Recently, Mortensen *et al.*²⁹ investigated both the dissociative chemisorption and associative desorption of CH₄ on Ru(0001). Using detailed balance arguments and a combination of molecular beam sticking and laser-induced associative desorption measurements, these authors presented a self-

Here $F(E, t)$ represents an external flux that forms PCs at energy E , $k_R(E)$ and $k_D(E)$ are microcanonical rate constants for reaction and desorption, and pseudo-first-order rate constants of the form $R(E, E')$ govern vibrational energy exchange with the substrate that transfers energetic PCs at energy E' to energy E . This equation reflects the additional assumption that when a gas molecule initially collides with the surface full statistical energy mixing occurs within the PC and the freely exchangeable or active energy E of the PC is

$$E = E_t + E_v + E_r + E_s + E_{ad}, \quad (2)$$

where E_s is the vibrational energy of s local surface oscillators, E_t , E_v , and E_r are the translational, vibrational, and rotational energies of the incident molecule, respectively, and E_{ad} is the adsorption energy. The energies that appear in Eq. (2) are understood to correspond to the active degrees of freedom of the PC, i.e., those that can freely contribute energy to surmount the threshold energies to dissociation and desorption, subject to applicable conservation laws.

Dissociative chemisorption studies of methane incident on Pt(111) have found that methane dissociative sticking scales with the normal component of the molecular translational energy, $E_n = E_t \cos^2 \vartheta$, where ϑ is the angle of incidence away from the surface normal. This “normal energy” scaling suggests that parallel momentum is conserved over the time scale of a reactive collision on the Pt(111) surface and that only the normal translational energy is effective in promoting reaction. For systems obeying normal energy scaling only the normal component of translational energy, E_n , contributes to E as E_t in Eq. (2).

The external flux that supplies PCs to the surface, $F(E, t)$, is the product of the total molecular flux incident on the surface, F_0 , and the probability distribution for creating a PC at energy E , $f(E)$, such that $F(E, t) = F_0 f(E)$. The $f(E)$ flux distribution is formed by convolution over the energy distribution functions for the flux-weighted translational, vibrational, and rotational energies of the incident molecule, along with the energy distribution for the s surface oscillators vibrating at the mean phonon frequency of the metal [$\nu_s = (\frac{3}{4})k_B \theta_{\text{Debye}}/h$ yielding 122 cm^{-1} for Pt(111)],

$$f(E) = \int_0^{E-E_{ad}} f_t(E_t) \int_0^{E-E_{ad}-E_t} f_v(E_v) \int_0^{E-E_{ad}-E_t-E_v} f_r(E_r) \times f_s(E-E_{ad}-E_t-E_v-E_r) dE_r dE_v dE_t. \quad (3)$$

For molecules incident from an ambient gas in thermal equilibrium with the surface, these distributions are canonical and characterized by a common temperature $T = T_g = T_s$.

The microcanonical rate constants for dissociation and desorption, $k_R(E)$ and $k_D(E)$, are of the Rice-Ramsperger-Kassel-Marcus (RRKM) form,⁴³

$$k_i(E) = \frac{W_i^\ddagger(E - E_i)}{h\rho(E)}, \quad (4)$$

where W_i^\ddagger is the sum of states for transition state i , E_i is the threshold energy for the i th reaction channel, h is Planck's

constant, and ρ is the PC density of states. Details concerning our choices of the transition states and reaction coordinates for CH_4 dissociation and desorption on Pt(111) are given in an earlier paper.²² Briefly, the desorption transition state is taken to occur when CH_4 is freely rotating and vibrating in the gas phase, far from the surface. The dissociation transition state is characterized by the nine vibrational modes of CH_4 in the gas, s vibrational modes of the Pt surface oscillators, four vibrational modes at a single lumped frequency, ν_D , representative of the three frustrated rotations and the vibration along the surface normal of methane at the dissociation transition state, and one of the triply degenerate antisymmetric C–H stretching vibrations ($\nu_3 = 3020 \text{ cm}^{-1}$) of CH_4 is sacrificed as the reaction coordinate.

When vibrational energy transfer between the PCs and the surrounding solid is neglected [i.e., the energy transfer integral of Eq. (1) is set to 0] the ME-MURT simplifies to the PC-MURT which only has three adjustable parameters, $\{E_0, \nu_D, s\}$, that can be fixed by comparative simulation to various experimental data. Best agreement of PC-MURT simulations to diverse CH_4 experiments on clean Pt(111) led to $\{E_0 = 0.61 \text{ eV}, \nu_D = 110 \text{ cm}^{-1}, s = 3\}$ parameters and a methane adsorption energy of $E_{ad} = 0.163 \text{ eV}$.²² These values are used throughout this paper to describe CH_4 dissociative chemisorption on clean Pt(111) and also serve to define $E_R = E_0 + E_{ad} = 0.773 \text{ eV}$ and $E_D = E_{ad} = 0.163 \text{ eV}$.

Vibrational energy transfer between the PCs and the surrounding solid is governed by rate coefficients $R(E, E')$ which can be expressed as the product of the total inelastic collision frequency, ω , and the collision step-size distribution, $P(E, E')$, as $R(E, E') = \omega P(E, E')$.⁴⁴ Although this separation of $R(E, E')$ is purely artificial, it does provide a useful physical picture for the energy transfer and a connection to vibrational energy transfer studies in the gas phase. With a consistent choice for the inelastic collision frequency, the collision step-size distribution is constrained by the requirements of detailed balance and normalization. Detailed balancing of the upward and downward rates of collisional energy transfer for an equilibrium population of PCs at the surface temperature ensures that the master equation provides for no net collisional energy transfer for a distribution of PCs in thermal equilibrium with the surface. Normalization of the collision step-size distribution guarantees that transitions from energy E' to all energies E occur with unit probability. Consequently, the ME-MURT of Eq. (1) can be simplified to

$$\frac{d\theta_p(E, t)}{dt} = F(E, t) - \{k_R(E) + k_D(E) + \omega\}\theta_p(E, t) + \omega \int_0^\infty P(E, E')\theta_p(E', t) dE'. \quad (5)$$

A. Dissociative sticking coefficient

Within the framework of the reaction scheme of Fig. 1, the experimentally realized sticking coefficient in the steady-state approximation when a time-independent flux of gas-phase molecules is made incident on a clean surface is

$$S = \frac{1}{F_0} \int_0^\infty k_R(E) \theta_p^{ss}(E) dE, \quad (6)$$

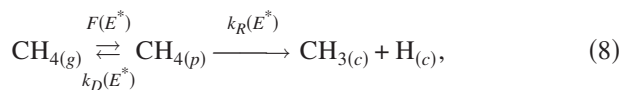
where $\theta_p^{ss}(E)$ is the steady-state coverage distribution of PCs and the integrand corresponds to the reactive flux for dissociative chemisorption. Applying the steady-state approximation to master equation (5), a formal solution for $\theta_p^{ss}(E)$ is

$$\theta_p^{ss}(E) = \frac{F_0 f(E) + \omega \int_0^\infty P(E, E') \theta_p^{ss}(E') dE'}{\omega + k_R(E) + k_D(E)}. \quad (7)$$

Although not a particularly useful expression for computing $\theta_p^{ss}(E)$, the numerator shows that for an arbitrary collision step-size distribution the steady-state distribution can be decomposed into a direct contribution from initial gas-surface collisions and an indirect contribution from PCs undergoing energy exchange with the surface. In addition, the denominator correctly shows that there are three ways for a PC to decay: dissociation, desorption, or energy exchange with the surface.

B. PC-MURT theoretical model

Neglecting the effects of vibrational energy exchange on the coverage distribution of PCs [e.g., by setting $\omega=0$ in Eq. (5)], the dissociative chemisorption kinetics of methane can be described microcanonically as



where the E^* zero of energy occurs with methane at infinite separation from the surface when all species are at 0 K,

$$E^* = E_t \cos^2 \vartheta + E_v + E_r + E_s. \quad (9)$$

Here we have explicitly included only the normal component of the molecular translational energy because the dissociative sticking coefficient of methane on Pt(111) is known to obey normal energy scaling. The steady-state approximation applied to the $\text{CH}_{4(p)}$ coverage of Eq. (8) yields a PC-MURT model that predicts

$$S = \int_0^\infty S(E^*) f(E^*) dE^*, \quad (10)$$

for the dissociative sticking coefficient where $S(E^*)$ is the microcanonical sticking coefficient defined by

$$S(E^*) = \frac{k_R(E^*)}{k_R(E^*) + k_D(E^*)} = \frac{W_R^\ddagger(E^* - E_R)}{W_R^\ddagger(E^* - E_R) + W_D^\ddagger(E^*)}, \quad (11)$$

and $f(E^*)$ is the flux distribution for creating a PC at E^* ,

$$f(E^*) = \int_0^{E^*} f_t(E_t) \int_0^{E^* - E_t} f_v(E_v) \int_0^{E^* - E_t - E_v} f_r(E_r) \times f_s(E^* - E_t - E_v - E_r) dE_r dE_v dE_t. \quad (12)$$

The construction of the microcanonical sticking coefficient from the RRKM rate constants for dissociation and desorption for the $\text{CH}_4/\text{Pt}(111)$ system is illustrated in Fig. 2 where the energy scale is $E = E^* + E_{ad}$. Following Eq. (6), separation of the integrand of Eq. (10) into the product of a coverage

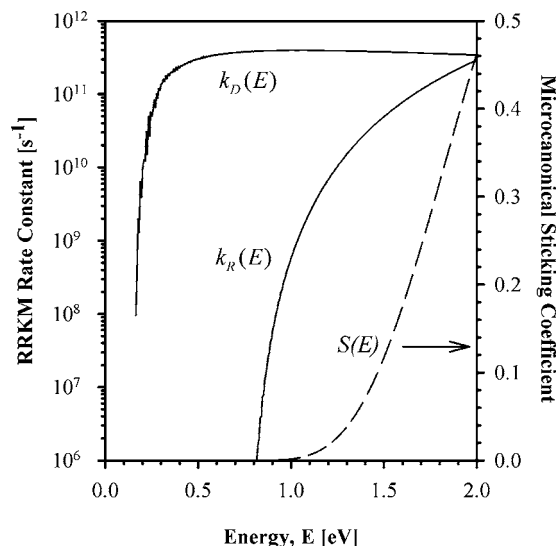


FIG. 2. Unimolecular rate constants [$k(E)$] for desorption and reaction of CH_4 on Pt(111). The microcanonical sticking coefficient, $S(E) = k_R(E) / [k_R(E) + k_D(E)]$, is plotted on a linear scale.

distribution and microcanonical rate constant for dissociation, we have for the PC-MURT steady-state coverage distribution,

$$\theta_p^{ss}(E^*) = \frac{F_0 f(E^*)}{k_R(E^*) + k_D(E^*)}, \quad (13)$$

a result which can also be obtained by setting $\omega=0$ in Eq. (7).

In summary, the PC-MURT approximation effectively treats each collisionally and transiently formed PC system of Fig. 1 as being adiabatically isolated from the surrounding metal heat reservoir and the E^* energy is assumed to be instantly microcanonically randomized over all active states of the PC for which energy can be freely exchanged. The sticking is independent of E_{ad} and the lack of vibrational energy exchange between the PCs and the surrounding metal does not allow for negative E^* .

III. VIBRATIONAL ENERGY EXCHANGE WITH THE SURROUNDING SOLID

Although there is a long history of investigation of vibrational energy transfer in bimolecular gas-phase collisions,⁴⁴ relatively little is known about the detailed form that the collision step-size distribution should take in gas-surface collisions. Previously, we suggested the density weighted exponential down model,²²

$$P(E, E') = \frac{\rho(E)}{N(E')} \exp\left\{-\frac{E' - E}{\alpha}\right\} \quad \text{for } E' > E, \quad (14)$$

where $N(E')$ is a normalization factor, $\rho(E)$ is the PC density of states, and α is a parameter closely approximating the average energy transferred in downward collisions, as a conceptually simple and easy to implement collision step-size distribution for which the exponential dependence of the energy transfer probability on the energy gap can be broadly rationalized on the basis of both classical and quantum mechanical analyses of intermolecular collisions. Using this

model for the collision step-size distribution and assuming a phonon-mediated energy exchange process (such that $\alpha = h\nu_s$ and $\omega = 3\nu_s$; which likely constitute upper bounds), ME-MURT modeling of *hyperthermal* supersonic molecular beam dissociative sticking coefficients of CH₄ on Pt(111) shows that inclusion of vibrational energy exchange yields sticking coefficients that differ insignificantly ($\pm 10\%$ at most) from those calculated using the PC-MURT.²²

In this section, we demonstrate that neglect of vibrational energy transfer is also a good approximation for the *thermal* dissociative sticking of methane on Pt(111) and illustrate the modest effect of energy transfer by considering two limiting cases: the PC-MURT (representing the absence of energy transfer) and the canonical strong collision ME-MURT (representing facile energy transfer) in the limit that the inelastic collision frequency is taken to infinity [i.e., is much greater than either $k_R(E)$ or $k_D(E)$]. In addition, we introduce for the first time the surface ergodic collision theory (SECT) of vibrational energy exchange between PCs and the surface as the limit of maximal energy transfer that is more physical than the canonical strong collision assumption and is fully consistent with the microcanonical mixing assumed in the initial gas-surface collision of the PC-MURT. A prescription for fixing parameters for a more realistic model of vibrational energy exchange at the surface [e.g., Eq. (14)] based on the SECT is developed and implemented. Bounds on the thermal dissociative sticking coefficient based on the limiting energy transfer models are established.

The simplest representation of the collision step-size distribution consistent with the requirements of normalization and detailed balance is the canonical strong collision assumption (SCA) which assumes that the collision step-size distribution is proportional to the equilibrium distribution of the final state and independent of the initial state.⁴⁵ Applied to the MURT, the SCA collision step-size distribution is given by the Boltzmann equilibrium distribution of PCs at the surface temperature, $B_p(E; T_s)$,

$$P^{\text{SCA}}(E, E') = B_p(E; T_s), \quad (15)$$

implying that a single collisional event thermally equilibrates energized PCs to the surface temperature. Although a physically implausible representation of collisional energy transfer, the SCA has been used extensively in the gas phase to fit experimental unimolecular falloff data through the introduction of an additional parameter called the collision efficiency that quantifies the degree of collisional weakness (i.e., departure from canonical strong collision behavior).⁴⁶ Part of the attractiveness of the SCA in the gas phase is that it allows for analytic solution of the master equation for unimolecular decomposition, providing a convenient formula that interpolates between the low and high pressure limits of the rate constant. In addition, the SCA correctly represents the ultimate effect of all collisional energy transfer mechanisms which is to drive a nonequilibrium reactant population towards thermal equilibrium (as expressed in the detailed balance constraint on the collision step-size distribution).

In analogy to the gas phase where the high pressure SCA leads to an upper bound on the rate constant for a unimolecular decomposition and weak collisions result in the

typical pressure dependent falloff behavior because the Boltzmann distribution of reactant species is difficult to maintain, within the MURT gas-surface reactivity model the infinite inelastic collision frequency strong collision (IFSC) limit provides an outer bound (in this case either a maximum or a minimum) on the range of thermal dissociative sticking possible for CH₄ on Pt(111) and, in addition, is analytically solvable. The PC-MURT provides the complementary outer bound on the possible range of the thermal sticking for a given set of transition state parameters $\{E_0, \nu_D, s\}$. Starting with Eq. (7), the strong collision solution to the master equation in steady state is

$$\theta_p^{\text{ss}}(E) = \frac{F_0 f(E) + \omega B_p(E; T_s) \int_0^\infty \theta_p^{\text{ss}}(E') dE'}{\omega + k_R(E) + k_D(E)}. \quad (16)$$

The Boltzmann distribution for the collection of oscillators that define the PC is

$$B_p(E; T_s) = \frac{\rho_\nu(E)}{Q_\nu} \exp\left(-\frac{E}{k_B T_s}\right), \quad (17)$$

where $\rho_\nu(E)$ is the vibrational density of states and Q_ν is the vibrational partition function. The PC is assumed to have the nine vibrational modes of gas-phase methane, four modes at ν_D that evolved from the incident CH₄ normal translation and three rotations, and s modes at the mean Pt phonon frequency ν_s (122 cm⁻¹). The values of ν_D and s are assumed to be the same as for the reactive transition state whose $\{E_0 = 0.61$ eV, $\nu_D = 110$ cm⁻¹, $s = 3\}$ characteristics have been defined by prior PC-MURT analysis²² of various CH₄/Pt(111) molecular beam experiments.

In the limit of infinite inelastic collision frequency ($\omega \rightarrow \infty$) Eq. (16) simplifies to

$$\theta_p^{\text{ss}}(E) = B_p(E; T_s) \int_0^\infty \theta_p^{\text{ss}}(E') dE' = \Theta_p^{\text{ss}} B_p(E; T_s), \quad (18)$$

where the total PC coverage in the steady state is defined as

$$\Theta_p^{\text{ss}} = \int_0^\infty \theta_p^{\text{ss}}(E') dE', \quad (19)$$

which can be calculated numerically²² by the steady-state solution of Eq. (5) in the limit that $\omega \gg k_D$ or k_R (e.g., $\omega = 10^{25}$ s⁻¹). Equation (18) shows that the steady-state PC coverage distribution is proportional to the equilibrium Boltzmann distribution in the IFSC limit. Note that Eqs. (16) and (18) bear resemblance to theories of precursor-mediated chemisorption such as Weinberg's treatment of thermalized trapping mediated dissociative chemisorption wherein a dynamical fraction of the incident molecular flux sticks to the surface and immediately thermally accommodates such that thermal Arrhenius rate constants are used thereafter to derive sticking probabilities.⁴⁷ Thus, although the IFSC limit may be unphysical, it appears to find a common use even in surface kinetics.⁴⁸

The limit of no energy transfer is represented by the PC-MURT [i.e., the ME-MURT of Eq. (5) with $\omega = 0$] wherein the initially formed PCs are not allowed to fall into the physisorption potential well and become thermalized to the surface temperature prior to dissociation or desorption

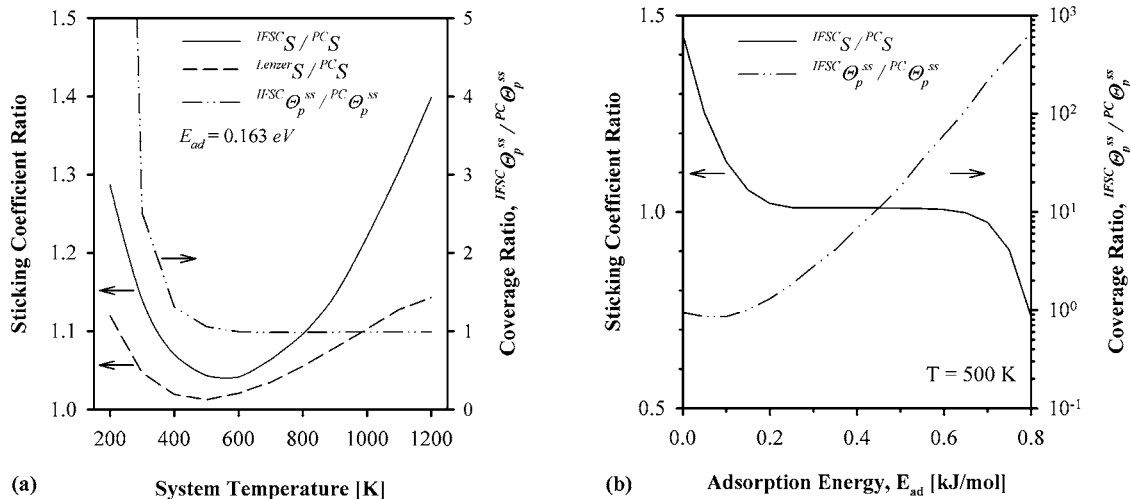


FIG. 3. (a) Comparison of the IFSC ME-MURT and Lenzel ME-MURT predicted thermal dissociative sticking coefficients to the PC-MURT predictions as the ratios $IFSC_S/PC_S$ and $Lenzeler_S/PC_S$. The thermal PC_S as a function of temperature is plotted in Fig. 14(a) of Ref. 22. The Lenzel $P(E, E')$ with $\omega = 3\nu_s$ is a more realistic vibrational energy transfer model and results in sticking that falls between the bounds set by the IFSC ME-MURT and PC-MURT. The steady-state coverage $IFSC\Theta_p^{ss}/PC\Theta_p^{ss}$ ratio is also plotted. (b) Comparison of the IFSC ME-MURT to PC-MURT predicted thermal dissociative sticking coefficients and steady-state coverages as the adsorption energy alone is allowed to vary at 500 K.

[see Eq. (13) and Fig. 1]. Although it is tempting to assume that the PC-MURT would represent the upper limit on the dissociative sticking coefficient because it has an energetic advantage of E_{ad} on the ME-MURT energy floor, regardless of the specific form of the collision step-size distribution, computation of the thermal dissociative sticking coefficient of CH_4 on Pt(111) between 200 and 1200 K for the IFSC ME-MURT and the PC-MURT shows that $IFSC_S > PC_S$ [see Fig. 3(a)]. However, over this range of temperatures, the differences between these two limiting energy transfer models do not significantly alter the sticking ($\leq 40\%$). At 200 K the computed $IFSC_S$ is only 29% larger than the PC_S , dropping to 4% larger at 500 K, and then rising to 40% larger at 1000 K.

For comparative purposes, it will prove useful to rewrite the steady-state dissociative sticking coefficient of Eq. (6) as

$$S = \frac{\Theta_p^{ss}}{F_0} \int_{E_R}^{\infty} k_R(E) \bar{\theta}_p^{ss}(E) dE, \quad (20)$$

where E is measured from the bottom of the physisorption potential well, Θ_p^{ss} is the total PC coverage defined by Eq. (19), and $\bar{\theta}_p^{ss}(E) = \theta_p^{ss}(E)/\Theta_p^{ss}$ is the normalized steady-state PC coverage distribution. This expression highlights that when comparing sticking coefficients from models generating different $\bar{\theta}_p^{ss}(E)$ two effects must be taken into account: the total PC coverage and the normalized coverage distribution at energies above the threshold to dissociation (i.e., $E > E_R$). The ME-MURT vibrational energy exchange allows for relaxation of some of the PC population into the physisorption potential well from where, upon each energy transfer event (e.g., $\omega \rightarrow \infty$ for the IFSC), these PCs may, according to their $P(E, E')$, repopulate PCs at reactive energies which have been lost due to desorption or dissociative chemisorption. In steady state for the thermal $CH_4/Pt(111)$ system, the IFSC ME-MURT is found to maintain greater total coverage, $IFSC\Theta_p^{ss}$, than the PC-MURT, $PC\Theta_p^{ss}$, for temperatures below about 500 K [Fig. 3(a)]. If at 500 K the

adsorption energy alone is increased, the $IFSC\Theta_p^{ss}$ increases but eventually this cannot compensate for the increase in $E_R = E_0 + E_{ad}$ and the $IFSC_S/PC_S$ sticking ratio falls below 1 [Fig. 3(b)]. In general, and dependent on the value of E_{ad} , it is possible for either the PC-MURT or the IFSC ME-MURT to provide an upper bound on the thermal dissociative sticking coefficient for fixed values of the three PC-MURT transition state parameters, $\{E_0, \nu_D, s\}$.

The thermal dissociative sticking coefficient calculated by the IFSC ME-MURT provides a limiting value consistent with infinitely fast vibrational energy exchange between the PCs and the surface that results in prompt thermalization of the PCs to the surface temperature. Thus, weaker forms of the collision step-size distribution, such as the Lenzel $P(E, E')$ of Fig. 3(a), will predict thermal dissociative sticking coefficients that fall between the limits set by the PC-MURT (no energy exchange) and the IFSC ME-MURT (instantaneous thermalization).

In passing, it is worth noting that for nonequilibrium dissociative chemisorption of *hyperthermal* methane molecules (e.g., in molecular beam experiments) the PC-MURT always provides an upper bound²² on the dissociative sticking coefficient because any vibrational energy transfer model that obeys detailed balance will yield a net downwards energy transfer that will tend to reduce the sticking towards the thermal equilibrium value.

A. Effect of the adsorption energy

The PC-MURT can be formulated entirely on the E^* energy scale of Eqs. (8)–(13) and so its sticking is independent of the value of E_{ad} . Under thermal equilibrium conditions, the IFSC ME-MURT sticking can be either greater or less than the PC-MURT sticking depending on the value of E_{ad} , as shown in Fig. 3(b). The reason for this is that a thermalized PC does not share exactly the same degrees of freedom as found in the thermal surface and incident gas-phase molecule prior to their PC forming collision.

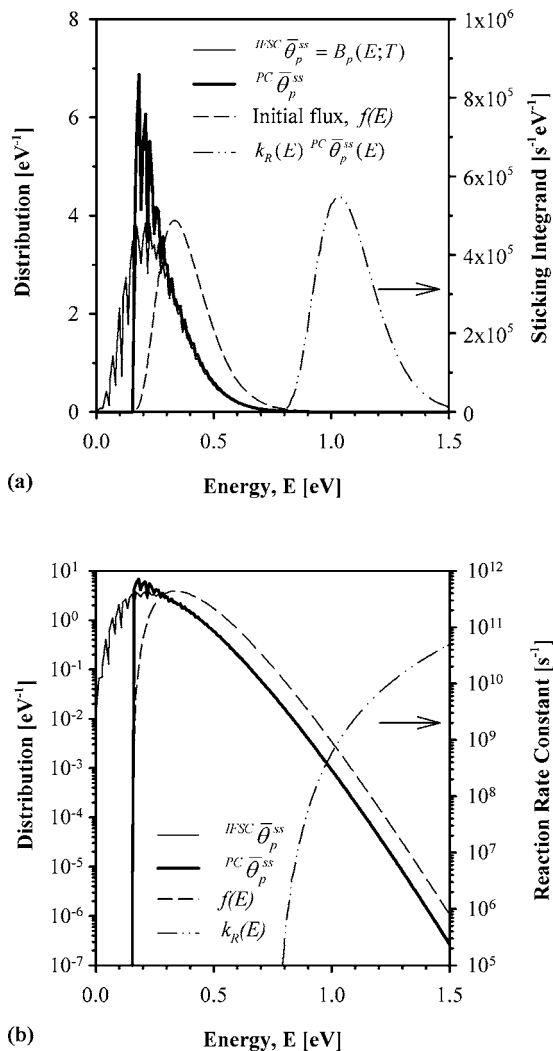


FIG. 4. Comparisons of the thermal PC-MURT and IFSC ME-MURT predicted steady-state physisorbed complex energy distributions and the initial flux distribution for CH₄ on Pt(111) at 500 K on (a) linear and (b) log scales. The sticking can be calculated as in Eq. (20), $S = \Theta_p^{ss} / F_0 \int_{E_R}^{\infty} k_R(E) \bar{\theta}_p^{ss}(E) dE$, where $E_{ad} = 0.163$ eV, $E_R = E_0 + E_{ad} = 0.773$ eV, $F_0 = 1$ ML/s, and the steady-state coverage is $\Theta_p^{ss} = (7.33 \pm 0.16) \times 10^{-10}$ ML. The Eq. (20) sticking integrand is plotted for the PC-MURT in (a) and the microcanonical reaction rate constant $k_R(E)$ is plotted in (b).

Figure 4 compares the IFSC ME-MURT and PC-MURT normalized PC coverage distributions for the CH₄/Pt(111) system at 500 K. The PC-MURT and IFSC ME-MURT predicted $\bar{\theta}_p^{ss}(E)$'s share similar mean energies, $\langle E \rangle_{ss} = 0.28 \pm 0.01$ eV. The distributions differ significantly up to energies near $E = 0.3$ eV, but by the reaction threshold energy ($E_R = 0.773$ eV) they are very similar. At these higher energies, the steady-state PC-MURT coverage distribution of Eq. (13) is $\bar{\theta}_p^{ss}(E) \approx f(E)/k_D(E)$ and $k_D(E)$ is approximately constant (see Fig. 2). Because the modes of the PCs are, for the most part, the same as those of the separated gas and surface oscillators that come together to form the PCs, at thermal equilibrium, the IFSC $\bar{\theta}_p^{ss}(E) = B_p(E; T)$ is similar to the PC flux distribution, $f(E = E^* + E_{ad})$, albeit that their natural energy floors are shifted by E_{ad} . The $\bar{\theta}_p^{ss}(E) \approx f(E)/k_D(E)$ just happens to be exceptionally similar to the IFSC $\bar{\theta}_p^{ss}(E) = B_p(E; T)$ at reactive energies

for the CH₄/Pt(111) kinetic parameters at 500 K. The integrand of the Eq. (20) sticking expression, $k_R(E) \bar{\theta}_p^{ss}(E)$, plotted in Fig. 4(a) for the PC-MURT, is proportional to the energy distribution of those PCs that successfully react.

Increasing E_{ad} alone at 500 K, as in Fig. 3(b), increases the energetic separation between the IFSC $\bar{\theta}_p^{ss}(E) = B_p(E; T)$ and $E_R = E_0 + E_{ad}$ and reduces the sticking integrand, $k_R(E) \bar{\theta}_p^{ss}(E)$. The congruent coverage increase as E_{ad} is increased can compensate for the reduced sticking integral in Eq. (20) over a limited range of E_{ad} but eventually the IFSC $S/PC S$ ratio sinks below 1.

In the limit that $E_{ad} \rightarrow 0$, the IFSC $\bar{\theta}_p^{ss}(E) = B_p(E; T)$ will be greater than $f(E)$ at reactive energies, as can be deduced from Fig. 4(b). This can be anticipated on the basis of classical equipartition because when thermal methane incident on the surface forms a PC which is subsequently thermalized, $k_B T$ of flux-weighted normal translation is exchanged for $k_B T$ of normal vibration and $(3/2)k_B T$ of rotational energy is exchanged for $3k_B T$ of “frustrated rotation” vibrational energy, since all other gas and surface modes are the same as within the PC and are prethermalized. The thermalized PC wins $(3/2)k_B T$ of energy with respect to the initially formed PC and hence the mean energy of $B_p(E; T)$ is higher than $f(E)$ when $E_{ad} = 0$. Furthermore, $B_p(E; T)$ extends to higher energy faster than $f(E)$ as the temperature is increased because the density of vibrational states rises faster with energy than the density of rotational states (since rotational state spacings increase with energy). The steady-state coverages IFSC $\bar{\theta}_p^{ss}(E) = B_p(E; T)$ and PC $\bar{\theta}_p^{ss}(E) \approx f(E)/k_D(E)$ within the Eq. (20) sticking integral are such that the IFSC $S/PC S$ sticking ratio is greater than 1 when $E_{ad} = 0$ and this ratio will increase as the temperature is increased. As E_{ad} is increased from 0, the IFSC ME-MURT sticking integral monotonically declines.

The interesting temperature functionality of IFSC $S/PC S$ displayed in Fig. 3(a) can now be more easily explained. At low temperatures (below about 500 K) the IFSC ME-MURT has greater total PC coverage compared to the PC-MURT. As the temperature increases the coverage advantage gained by “hiding” population in the physisorption potential well diminishes because a greater proportion is exposed to desorptive and reactive losses and the IFSC $S/PC S$ ratio falls. The IFSC $S/PC S$ curve minimum occurs at a temperature where the mean energies of the IFSC ME-MURT and PC-MURT coverage distributions are equal (near 500 K). As the temperature increases further the IFSC $\bar{\theta}_p^{ss}(E) = B_p(E; T)$ distribution moves towards higher energy faster than the PC $\bar{\theta}_p^{ss}(E) \approx f(E)/k_D(E)$ distribution and the IFSC $S/PC S$ ratio increases.

B. Surface ergodic collision theory

Collisional energy transfer cannot be expected to be as strong as the canonical strong collision assumption (SCA) proposes. Typically, in the gas phase, collisions are far from strong and are sufficiently infrequent as to be unable to sustain a Boltzmann distribution at energies far exceeding the threshold for reaction where reactant population is constantly depleted due to reaction. As a more physical alternative to

the canonical strong collision assumption we have formulated a surface ergodic collision theory (SECT) of collisional energy transfer based on the gas-phase bimolecular ergodic collision theory (ECT) of Nordholm *et al.*⁴⁹ This theory is essentially a microcanonical strong collision assumption based on the idea that transfer of an energized complex from initial energy E' to final energy E occurs through establishment of full microcanonical equilibrium (rather than the canonical equilibrium assumed in the SCA) between the active molecular and surface degrees of freedom followed by resamplings of the thermally populated ensemble of surface modes contributing to the physisorbed complex (PC).

An energized PC formed at initial energy E' and composed of ν active degrees of freedom, of which s are surface oscillators and p labels the remaining degrees of freedom, has the microcanonical probability

$$P(E_p|E') = \frac{\rho_p(E_p)\rho_s(E' - E_p)}{\rho_{ps}(E')}, \quad (21)$$

to have energy E_p in the p portion of the PC where $\rho_p(E_p)$ is the density of states of the p modes, $\rho_s(E_s)$ is the density of states of the s surface modes, and $E' = E_p + E_s$. Following this energy partitioning the ν - s degrees of freedom described by the energy E_p resample a thermal distribution of surface oscillators,

$$f_s(\varepsilon; T_s) = \frac{\rho_s(\varepsilon)e^{-\varepsilon/k_B T_s}}{Q_s(T_s)}, \quad (22)$$

to form the final energy $E = E_p + \varepsilon$ such that the collision step-size distribution for the SECT model is

$$\begin{aligned} P(E, E') &= \int_{\max(0, E-E')}^{E'} P(E_p|E') f_s(\varepsilon; T_s) d\varepsilon \\ &= Q_s(T_s)^{-1} \int_{\max(0, E-E')}^{E'} \frac{\rho_p(E - \varepsilon)\rho_s(E' - E + \varepsilon)}{\rho_{ps}(E')} \\ &\quad \times \rho_s(\varepsilon) e^{-\varepsilon/k_B T_s} d\varepsilon, \end{aligned} \quad (23)$$

where the limits of integration are set to obey conservation of energy. For the $\text{CH}_4/\text{Pt}(111)$ system, Fig. 5 shows the collision step-size distribution at reaction threshold (i.e., $E_R = E_0 + E_{\text{ad}} = 0.773$ eV) for the SECT energy transfer model as well as the average energy transferred in downward, upward, and all collisions. These average energy transfer quantities are defined as

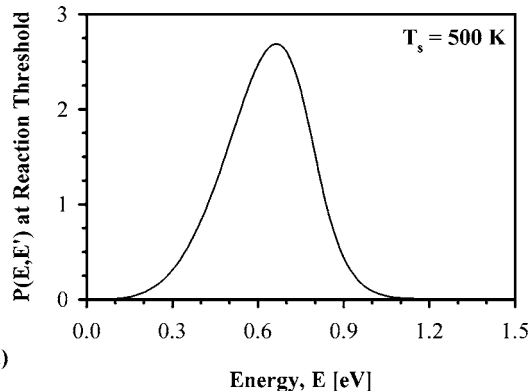
$$\langle \Delta E(E') \rangle_d = \int_0^{E'} (E' - E) P(E, E') dE \quad \text{for } E' > E, \quad (24)$$

$$\langle \Delta E(E') \rangle_u = \int_{E'}^{\infty} (E - E') P(E, E') dE \quad \text{for } E' < E, \quad (25)$$

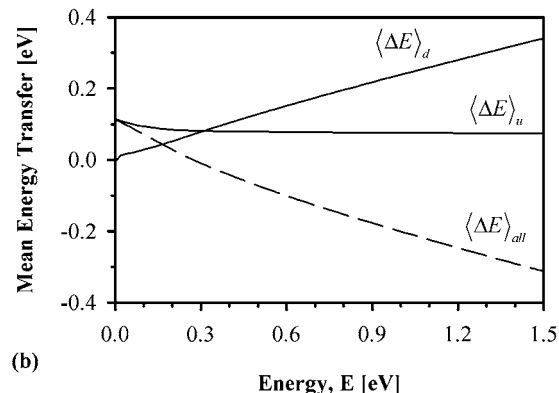
and

$$\langle \Delta E(E') \rangle_{\text{all}} = \int_0^{\infty} (E - E') P(E, E') dE, \quad (26)$$

respectively.



(a)



(b)

FIG. 5. Surface ergodic collision theory (a) collision step-size distribution at reaction threshold and (b) the average energies transferred in downward collisions $\langle \Delta E \rangle_d$, upward collisions $\langle \Delta E \rangle_u$, and all collisions $\langle \Delta E \rangle_{\text{all}}$ at 500 K surface temperature.

The validity of a microcanonical approach to intermolecular energy transfer has been verified in the gas phase by Nordholm and co-workers,^{50,51} with their development of the partially ergodic collision theory (PECT) to account for the weakness of the observed collisional energy transfer compared to that predicted by the ECT. Quantifying the degree of collisional weakness through an energy transfer efficiency parameter β_E defined as

$$\beta_E = \frac{\langle \Delta E \rangle_{\text{all}}^{\text{observed}}}{\langle \Delta E \rangle_{\text{all}}^{\text{ECT}}}, \quad (27)$$

where $\langle \Delta E \rangle_{\text{all}}^{\text{observed}}$ and $\langle \Delta E \rangle_{\text{all}}^{\text{ECT}}$ are the average energies transferred in all collisions observed in the experiment and computed with the ECT, respectively. They found that for toluene and azulene with a wide range of colliders and collision energies, β_E was approximately 0.1. Despite the order of magnitude difference between the observed and ECT prediction of the average energy transferred in the collisions, the stability of β_E around 0.1 was taken as a strong indicator of the fundamental role of statistical energy mixing mechanisms in gas-phase collisional energy transfer. The PECT model was developed as an interpretation of this observed weakness of collisional energy transfer in terms of active and inactive subsets of degrees of freedom and reproduces the experimentally observed collision step-size distributions for toluene and azulene very well.

Although it is possible to formulate a surface version of the gas-phase PECT, the resultant equations are quite cum-

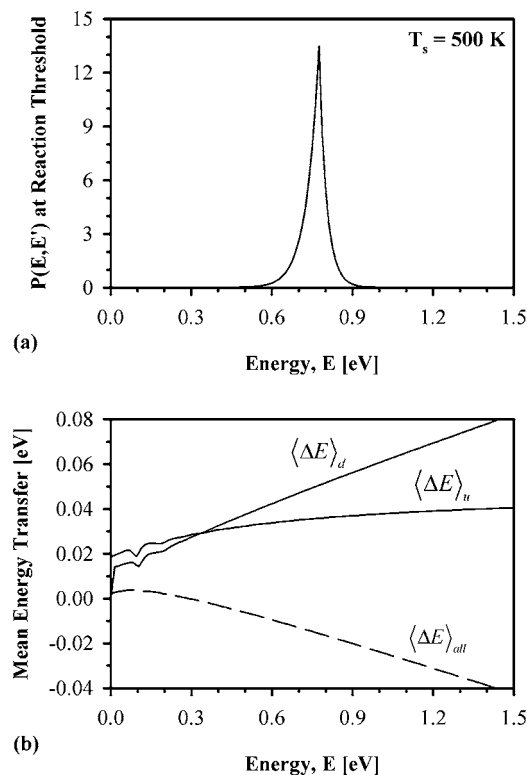


FIG. 6. Generalized density weighted exponential down (a) collision step-size distribution at reaction threshold and (b) the average energies transferred in downward collisions $\langle \Delta E \rangle_d$, upward collisions $\langle \Delta E \rangle_u$, and all collisions $\langle \Delta E \rangle_{all}$ at 500 K surface temperature with $c_0=50 \text{ cm}^{-1}$, $c_1=0.1$, and $\gamma=1$.

bersome and rather than attempt its implementation we have again followed the lead of Nordholm and co-workers in the gas phase and instead implemented a version of the “monoexponential form with a parametrized exponent” of Lenzer *et al.*⁵² as an excellent alternative to the PECT.^{50,51} Our density weighted exponential down model with a parametrized exponent is

$$P(E, E') = \frac{\rho(E)}{N(E')} \exp \left\{ - \left| \frac{E' - E}{c_0 + c_1 E'} \right|^\gamma \right\}, \quad (28)$$

where c_0 , c_1 , and γ are constants chosen such that the average energy transferred in all collisions at reaction threshold is some fraction of the SECT value, in this instance 10%, leading to $c_0=50 \text{ cm}^{-1}$, $c_1=0.1$, and $\gamma=1$. In this manner, and in analogy to the development of PECT for the gas phase by Nordholm and co-workers,^{50,51} a presumably realistic $P(E, E')$ for surface energy transfer may be defined without the need for prior experimental information and with minimal parametrization (e.g., by requiring $\langle \Delta E(E') \rangle_{all}$ to be 10% of the SECT value). The “Lenzer” collision step-size distribution derived from this procedure is given in Fig. 6 at reaction threshold along with the average energy transfer quantities defined by Eqs. (24)–(26). An interesting aspect of the average energy transferred in all collisions is that it is positive at energies less than about 0.25 eV. This could have implications for the fitting of molecular beam dissociative chemisorption data that shows an initial decrease in sticking with increasing translational energy followed by a monotonic increase with translational energy, e.g., for the methane/

Ir(111) system.²⁷ However, for the thermal sticking of methane on Pt(111) this Lenzer form of the collision step-size distribution is weaker than the SCA model and with $\omega=3\nu_s$ predicts sticking coefficients intermediate to those of the PC-MURT and IFSC ME-MURT, as shown in Fig. 3(a). Finally, it should always be kept in mind that the nonequilibrium molecular beam experiments clearly demonstrate that the initial translational¹⁸ and internal⁴ energies of the incident methane play important roles in dictating dissociative sticking coefficients and so the $\omega \rightarrow \infty$ IFSC ME-MURT energy transfer limit (i.e., instantaneous memory loss and thermal equilibration of all PC modes to T_s) is never realized in nature.

IV. DISSOCIATIVE STICKING AT THERMAL EQUILIBRIUM

Having demonstrated the minimal effect of vibrational energy transfer between the initially formed PCs and the surrounding substrate for the thermal dissociative chemisorption of CH_4 on a clean Pt(111) surface, we now use the PC-MURT to derive molecular energy distributions appropriate to the thermal dissociative methane flux and, by detailed balance, the product methane flux from associative desorption (treated in Sec. V). The total reactive flux in dissociative chemisorption, D_0 , is the product of the total molecular flux incident on the surface, F_0 , and the total sticking coefficient, S , such that,

$$D_0 = SF_0, \quad (29)$$

and

$$D(E_t, E_v, E_r) = S(E_t, E_v, E_r)F(E_t, E_v, E_r), \quad (30)$$

where Eq. (30) is simply a microscopically detailed version of Eq. (29). Defining $\xi(E_t, E_v, E_r)$ as the normalized molecular energy distribution of those incident molecules that go on to react, for specific molecular parameters the dissociative chemisorption reactive flux is

$$D(E_t, E_v, E_r)dE_t dE_v dE_r = D_0 \xi(E_t, E_v, E_r)dE_t dE_v dE_r. \quad (31)$$

Likewise, the total molecular flux incident on the surface is

$$F(E_t, E_v, E_r)dE_t dE_v dE_r = F_0 f_m(E_t, E_v, E_r)dE_t dE_v dE_r, \quad (32)$$

where $f_m(E_t, E_v, E_r)$ is the normalized molecular energy distribution of all molecules incident on the surface. Combining Eqs. (29)–(32) the detailed energy distribution of the reactive flux is

$$\xi(E_t, E_v, E_r) = \frac{1}{S} S(E_t, E_v, E_r) f_m(E_t, E_v, E_r). \quad (33)$$

This distribution can be further specified by writing the molecular-energy-resolved sticking coefficient, $S(E_t, E_v, E_r)$, in terms of the microcanonical sticking coefficient, $S(E^*)$, via the canonical surface vibrational energy distribution, $f_s(E_s)$, as

$$S(E_t, E_v, E_r) = \int_0^\infty S(E^*) f_s(E_s) dE_s, \quad (34)$$

such that

$$\xi(E_t, E_v, E_r) = \frac{1}{S} f_t(E_t) f_v(E_v) f_r(E_r) \int_0^\infty S(E^*) f_s(E_s) dE_s, \quad (35)$$

where the energy distribution of the incident molecules, $f_m(E_t, E_v, E_r)$, is given by the product of canonical energy distributions for each degree of freedom at the common temperature $T = T_g = T_s$ of the system and the total thermal sticking coefficient is given by Eq. (10).

Except for the possibility of introduction through the microcanonical sticking coefficient from the definition of the active energy, an angular dependence is generally introduced into the reactive molecular energy distribution through the molecular translational energy distribution appropriate to a thermal ambient gas incident on a surface. This distribution is the flux-weighted Maxwell-Boltzmann (FWMB) distribution⁵³ and in spherical polar coordinates the probability for thermal incident molecules to have translational energy from E_t to $E_t + dE_t$ in solid angle $d^2\Omega(\vartheta, \varphi) = \sin \vartheta d\vartheta d\varphi$ is

$$\frac{d^3f}{dE_t \sin \vartheta d\vartheta d\varphi} = \frac{\cos \vartheta}{\pi} \frac{E_t}{(k_B T)^2} e^{-E_t/k_B T} = \frac{\cos \vartheta}{\pi} f_t(E_t), \quad (36)$$

where ϑ is measured with respect to the surface normal and normalization is over the forward hemisphere. For normal energy-scaled dissociative chemisorption systems, such as the methane/Pt(111) system, the flux-weighted distribution appropriate to the normal component of the incident translational energy can be found by transforming to the normal energy variable $E_n = E_t \cos^2 \vartheta$, and integrating Eq. (36) over the forward hemisphere of solid angles to obtain

$$f_n(E_n) = \frac{df_t}{dE_n} = \frac{1}{k_B T} e^{-E_n/k_B T}, \quad (37)$$

which has a mean energy of $k_B T$ as opposed to $2k_B T$ for the total FWMB translational energy distribution of Eq. (36). This distribution appears in the expression for the thermal sticking coefficient for normal energy-scaled systems,²²

$$S = \frac{1}{k_B T} \int_0^\infty S(E^*) \int_0^{E^*} f_{vrs}(E^* - E_n) e^{-E_n/k_B T} dE_n dE^*, \quad (38)$$

derived from Eqs. (10)–(12) where $f_{vrs}(E_{vrs})$ is defined below, and can often be used to simplify PC-MURT derived energy distributions. Replacing the general molecular translational energy distribution, $f_t(E_t)$, in our expression for the reactive molecular energy distribution with the FWMB distribution appropriate to thermal conditions introduces an explicit angular dependence and we write, more precisely than Eq. (35),

$$\xi(E_t, E_v, E_r, \vartheta) = \frac{\cos \vartheta}{\pi S} f_t(E_t) f_v(E_v) f_r(E_r) \times \int_0^\infty S(E^*) f_s(E_s) dE_s. \quad (39)$$

From this expression it is possible to calculate angle-dependent or angle-integrated probability distributions for each type of molecular energy (translational, vibrational, and rotational) as well as an expression for the angular dependence of the dissociative chemisorption yield.

The reactive translational energy distribution at an angle ϑ relative to the surface normal is obtained by integrating the detailed energy distribution of Eq. (39) over vibrational and rotational energies. Performing the integral over rotational energies using the substitution $E_{rs} = E_r + E_s$, we have

$$\begin{aligned} \xi(E_t, E_v, \vartheta) &= \frac{\cos \vartheta}{\pi S} f_t(E_t) f_v(E_v) \int_0^\infty f_r(E_r) \int_0^\infty S(E^*) f_s(E_s) dE_s dE_r \\ &= \frac{\cos \vartheta}{\pi S} f_t(E_t) f_v(E_v) \int_0^\infty S(E_t + E_v + E_{rs}) \\ &\quad \times \left\{ \int_0^{E_{rs}} f_r(E_{rs} - E_s) f_s(E_s) dE_s \right\} dE_{rs} \\ &= \frac{\cos \vartheta}{\pi S} f_t(E_t) f_v(E_v) \int_0^\infty S(E_t + E_v + E_{rs}) f_{rs}(E_{rs}) dE_{rs}, \quad (40) \end{aligned}$$

where $f_{rs}(E_{rs})$ is identified as the bracketed term of the second line. The integral over vibrational energy is performed in a similar fashion using the substitution $E_{vrs} = E_v + E_{rs}$ to obtain

$$\xi(E_t, \vartheta) = \frac{\cos \vartheta}{\pi S} f_t(E_t) S(E_t), \quad (41)$$

where the translational energy-resolved sticking coefficient, $S(E_t)$ is defined as

$$S(E_t) = \int_0^\infty S(E_t + E_{vrs}) f_{vrs}(E_{vrs}) dE_{vrs}. \quad (42)$$

In this equation $f_{vrs}(E_{vrs})$ is the convolution of the molecular vibrational, molecular rotational, and surface vibrational energy distributions.

Let us now specialize to reactive systems such as $\text{CH}_4/\text{Pt}(111)$ that exhibit normal energy scaling that is symmetric about the azimuthal angle, such that Eq. (41) becomes

$$\xi(E_t, \vartheta) = \frac{\cos \vartheta}{\pi S} f_t(E_t) S(E_t \cos^2 \vartheta). \quad (43)$$

Integration of this equation over the forward hemisphere to obtain the angle-integrated reactive translational energy distribution can be performed in one of the two essentially equivalent ways. Working with the total translational energy and integrating Eq. (41) over the appropriate solid angles using the substitution $E_n = E_t \cos^2 \vartheta$ yields

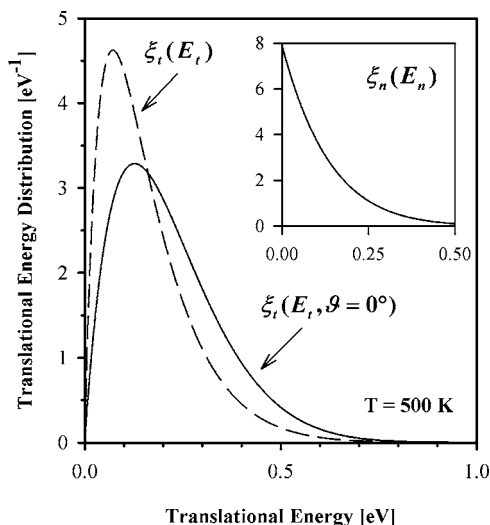


FIG. 7. PC-MURT translational energy distributions of the normally incident, $\xi_t(E_t, \vartheta=0^\circ)$, and angle-integrated, $\xi_t(E_t)$, reactive thermal CH_4 flux on Pt(111) at 500 K for $E_0=0.61$ eV. The angle-integrated normal translational energy distribution of the reactive flux, $\xi_n(E_n)$, under the same conditions is given in the inset (same axis labels).

$$\xi(E_t) = \frac{e^{-E_t/k_B T}}{(k_B T)^2 S} \int_0^{E_t} S(E_n) dE_n. \quad (44)$$

In the limit that S and $S(E_n) \rightarrow 1$, Eq. (42) simply recovers the *angle-integrated* FWMB translational energy distribution of Eq. (36). On the other hand, transforming to the normal component of translational energy prior to integrating yields the following expression for the distribution of normal translational energy:

$$\xi(E_n) = \frac{S(E_n)}{S} f_n(E_n), \quad (45)$$

where

$$S(E_n) = \int_0^\infty S(E_n + E_{vrs}) f_{vrs}(E_{vrs}) dE_{vrs}. \quad (46)$$

Similar expressions for the vibrational and rotational energies of the reacting molecules for normal energy-scaled systems can also be derived and are given by

$$\xi(E_v, \vartheta) = \frac{\cos \vartheta}{\pi S} f_v(E_v) S(E_v, \vartheta), \quad (47)$$

and

$$\xi(E_r, \vartheta) = \frac{\cos \vartheta}{\pi S} f_r(E_r) S(E_r, \vartheta), \quad (48)$$

respectively. In these equations the angular dependence of the molecular energy-resolved microcanonical sticking coefficients $S(E_v, \vartheta)$ and $S(E_r, \vartheta)$ derives from the angular dependence of the active energy [see Eq. (9)]. For example, $S(E_v, \vartheta)$ in Eq. (47) is

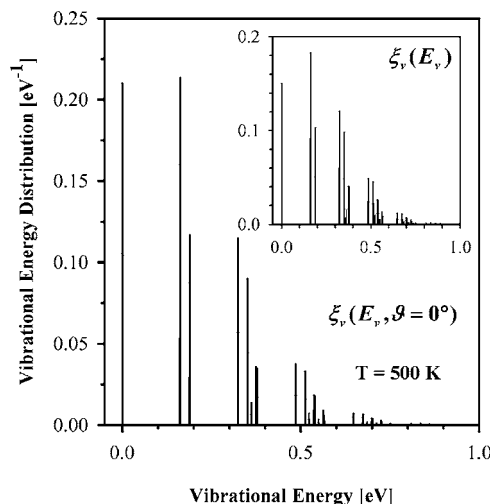


FIG. 8. PC-MURT vibrational energy distributions of the normally incident and angle-integrated (inset) reactive thermal CH_4 flux on Pt(111) at 500 K for $E_0=0.61$ eV.

$$S(E_v, \vartheta) = \int_0^\infty S(E_v + E_{trs}) f_{trs}(E_{trs}) dE_{trs}, \quad (49)$$

where $E_{trs} = E_t \cos^2 \vartheta + E_r + E_s$ and $f_{trs}(E_{trs})$ is the convolution of $f_t(E_t)$, $f_r(E_r)$, and $f_s(E_s)$,

$$f_{trs}(E_{trs}) = \int_0^{E_{trs}/\cos^2 \vartheta} f_t(E_t) \int_0^{E_{trs}-E_t \cos^2 \vartheta} f_r(E_r) f_s(E_{trs} - E_t \cos^2 \vartheta - E_r) dE_r dE_t. \quad (50)$$

Angular integration of Eq. (47) yields

$$\xi(E_v) = \frac{S(E_v)}{S} f_v(E_v), \quad (51)$$

where

$$S(E_v) = \int_0^\infty S(E_v + E_{nrs}) f_{nrs}(E_{nrs}) dE_{nrs}, \quad (52)$$

in which the subscript n designates the normal component of the translational energy and all other variables are defined as above. The rotational $\xi(E_r)$ and $S(E_r)$ are similarly constructed.

For thermal dissociative chemisorption of CH_4 on Pt(111) at 500 K system temperature Figs. 7–9 illustrate the above derived translational, vibrational, and rotational distributions of those incident molecules that go on to react, respectively. For the active degrees of freedom (i.e., E_n , E_v , E_r , and E_s) these reactive energy distributions are well described by reactant thermal distributions at an elevated effective temperature of 1350 K (Ref. 22) [n.b., such distributions can be explicitly compared in plots for the $\text{CH}_4/\text{Ni}(100)$ system¹⁴]. The effective temperature describing the reactive angle-integrated total translational energy distribution is somewhat lower at 925 K.

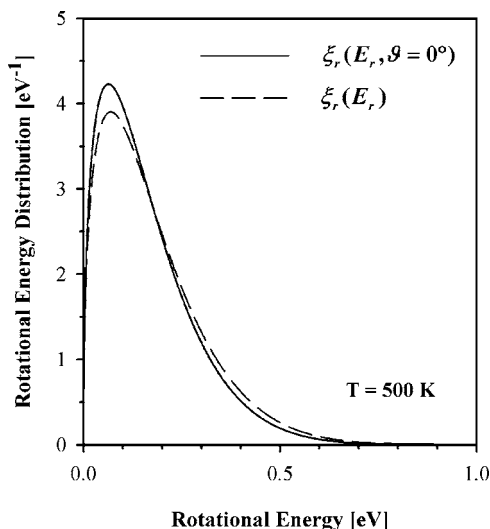


FIG. 9. PC-MURT rotational energy distributions of the normally incident and angle-integrated reactive thermal CH_4 flux on Pt(111) at 500 K for $E_0=0.61$ eV.

Figure 10 shows the angular variation of the mean energies of the reactive thermal CH_4 flux on Pt(111) at 500 K. These quantities are computed as

$$\langle E_i(\vartheta) \rangle_R = \frac{\int_0^\infty E_i \xi(E_i, \vartheta) dE_i}{\int_0^\infty \xi(E_i, \vartheta) dE_i}, \quad (53)$$

where the index i labels either t , v , r , or s . The mean normal translational energy of the reactive CH_4 is simply $\langle E_n(\vartheta) \rangle_R = \langle E_t(\vartheta) \rangle_R \cos^2 \vartheta$. Although the total mean active energy of the reactive PCs is fairly independent of the inci-

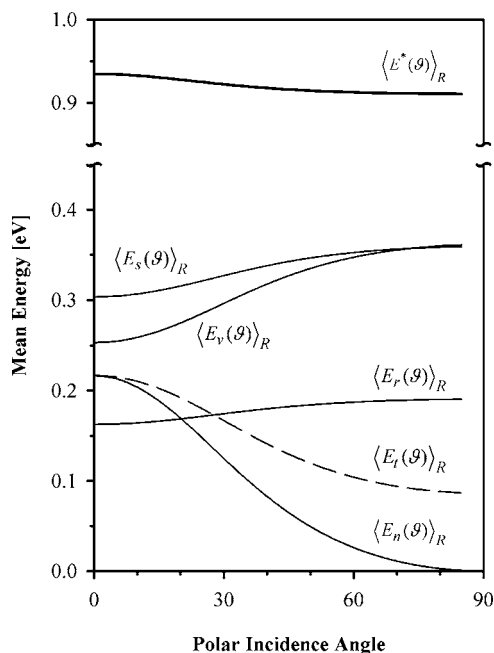


FIG. 10. Variation of the mean energies of the reactive thermal CH_4 flux on Pt(111) at 500 K for $E_0=0.61$ eV. The mean surface vibrational energy $\langle E_s(\vartheta) \rangle_R$, the mean CH_4 vibrational energy, the mean CH_4 rotational energy $\langle E_r(\vartheta) \rangle_R$, and the mean CH_4 normal translational energy $\langle E_n(\vartheta) \rangle_R$ contribute to the total active mean energy of the physisorbed complexes $\langle E^*(\vartheta) \rangle_R$. The total mean translational energy $\langle E_t(\vartheta) \rangle_R$ (dashed line) of the reacting CH_4 is also shown.

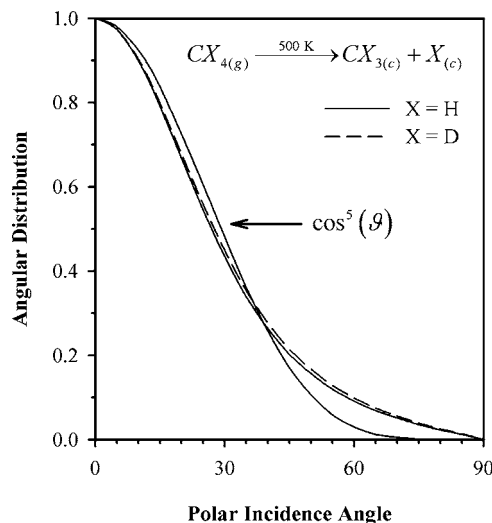


FIG. 11. PC-MURT angular distributions of the reactive thermal methane flux on Pt(111) at 500 K for $E_0=0.61$ eV. Both methane curves are best approximated by a $\cos^5 \vartheta$ distribution.

dence angle, energies from the surface and molecular vibrational and rotational motions contribute a larger proportion of the total mean energy as ϑ increases from 0° to 90° . This is compensated for by a decrease in the reactive CH_4 normal translational energy with an increasing angle of incidence.

For normal energy-scaled systems the angular distribution in dissociative chemisorption is derived by integrating Eq. (39) into a particular solid angle over the full range of molecular energies,

$$\xi(\vartheta) = \frac{\cos \vartheta}{\pi S} \int_0^\infty S(E^*) f_{\text{IVRS}}(E^*) dE^*, \quad (54)$$

where $f_{\text{IVRS}}(E_{\text{IVRS}})$ is the convolution [e.g., Eq. (50)] of $f_t(E_t)$, $f_v(E_v)$, $f_r(E_r)$, and $f_s(E_s)$ and $E_{\text{IVRS}} = E_t \cos^2 \vartheta + E_v + E_r + E_s$. Figure 11 shows the angular distribution of the reactive methane thermal flux on Pt(111) at 500 K. The best fit of these distributions to a $\cos^n \vartheta$ form yields $n=5$ in both cases. The decrease of the angular distribution with an increasing angle of incidence away from the surface normal is the result of the activated nature of this system. At a given temperature the large barrier to dissociation encountered by incident molecules is best surmounted at normal incidence when all of the molecules' translational energy is active.

In order to characterize energy consumption in the dissociative chemisorption of methane on Pt(111) we define differential energy uptake parameters, d_j , as

$$d_j \equiv \frac{\langle E_j \rangle_R - \langle E_j \rangle}{\langle E^* \rangle_R - \langle E^* \rangle} = \frac{\langle E_j \rangle_R - \langle E_j \rangle}{E_a}, \quad (55)$$

where $\langle E_j \rangle_R$ and $\langle E_j \rangle$ are the mean energies derived from the j th degrees of freedom of the molecules or surface that form reactive PCs and all PCs, respectively. Similarly, $\langle E^* \rangle_R$ and $\langle E^* \rangle$ are the mean total energies of the reactive PCs and all the PCs formed, respectively. For the $\text{CH}_4/\text{Pt}(111)$ system these quantities are shown in Fig. 12(a) as a function of temperature from 50 to 1000 K. Figure 12(b) shows the de-

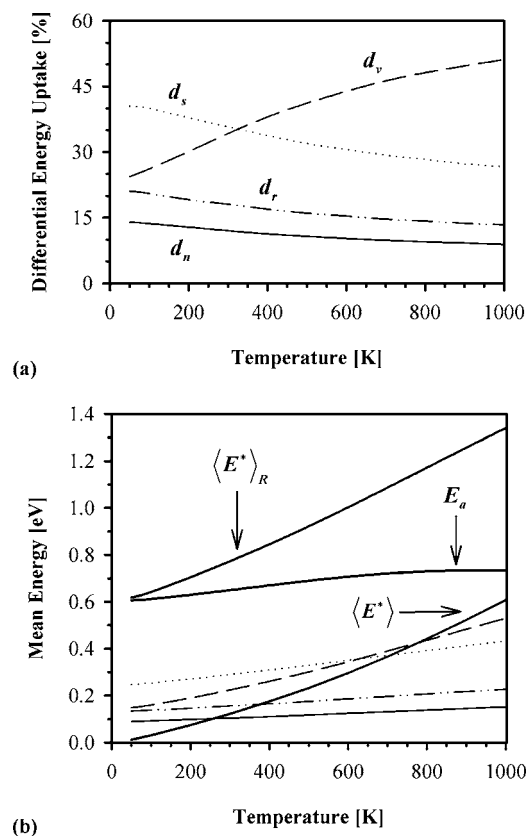


FIG. 12. Dissociative chemisorption of CH₄ on Pt(111) at thermal equilibrium: (a) differential energy uptakes and (b) mean energies derived from the j th degrees of freedom for physisorbed complexes undergoing reaction [the four bottom most lines are $\langle E_n \rangle_R$ (solid), $\langle E_r \rangle_R$ (dot dash), $\langle E_s \rangle_R$ (dashed), and $\langle E_v \rangle_R$ (dotted)]. Also shown in part (b) is the dependence of the activation energy, $E_a = \langle E^* \rangle_R - \langle E^* \rangle$, on temperature, where $E_a(T=0) = E_0 = 0.61$ eV.

pendence of the $\langle E_j \rangle_R$, $\langle E^* \rangle_R$, and $\langle E^* \rangle$ on temperature where the thermal activation energy is defined as²²

$$E_a(T) \equiv -k_B \frac{\partial \ln S}{\partial (1/T)} = \langle E^* \rangle_R - \langle E^* \rangle. \quad (56)$$

Over this range of temperatures the surface and molecular vibrational degrees of freedom contribute the most additional energy to the reacting PCs and are thus most important in promoting dissociative chemisorption. Within the statistical PC-MURT model it is the relative availability of different types of active energy to form PCs with sufficient pooled energy to react under given experimental conditions that is the key issue in dictating the differential energy uptakes. Certainly in the microcanonical theory, energy in any active degree of freedom is equally effective in helping to surmount the threshold energy to dissociative chemisorption so only the relative availability of the different types of energy can matter. Differential energy uptakes, rather than the fractional energy uptakes defined in a previous paper,²² are particularly instructive for the analysis of thermal dissociative chemisorption because it is the thermal activation energy, E_a , rather than the reaction threshold energy, E_0 , that is the average barrier that must be surmounted under thermal equilibrium conditions. Like the fractional energy uptakes, the differential energy uptakes sum to unity but give a better accounting

of whether one degree of freedom plays a particularly important role in aiding the PCs to surmount the temperature-dependent activation barrier. Figure 12 illustrates that at temperatures relevant to catalysis, $T > 500$ K, molecular vibrational energy is the most important energy source for surmounting the activation barrier. In PC-MURT simulations of the vibrational state-resolved dissociative chemisorption of methane on Ni(100),¹⁴ it was found that CH₄ sticking from the population of the fundamental and overtone of the highest degeneracy (threefold) and lowest energy (1305 cm⁻¹) ν_4 bending mode contributed most to the thermal sticking at 500 K. Clearly, it is the relative availability of energy from the different degrees of freedom that determines the differential energy uptakes.

V. METHANE ASSOCIATIVE DESORPTION FROM Pt(111)

Having treated the thermal dissociative chemisorption of methane on an initially clean Pt(111) surface, we now consider the application of the PC-MURT equations derived above to the reverse process of associative desorption. Following the kinetics of Fig. 1, we consider the CH_{4(g)} \rightleftharpoons CH_{3(c)} + H_(c) reactions to share a common adiabatic potential energy surface and equate the reactive methane flux in dissociative chemisorption with the product methane flux from the associative desorption of chemisorbed methyl and hydrogen using the principle of detailed balance at thermal equilibrium. Measurements of product methane flux distributions from associative desorption experiments could directly test the PC-MURT predictions if an appropriate thermal quasiequilibrium amongst the surface species can be maintained during desorption. This last condition is difficult to ensure because methyl radicals are known to competitively decompose on Pt(111) at temperatures appropriate to associative desorption.

Following detailed balance, the CH₄/Pt(111) molecular translational, vibrational, and rotational reactive energy distributions of Figs. 7–9 at 500 K system temperature are equivalent to the product flux distributions from associative desorption in the zero coverage limit where the threshold to dissociation is 0.61 eV. Although the normal translational energy distribution, $\xi(E_n)$, shown in the inset of Fig. 7 is a useful theoretical construct,¹⁴ it is not directly observable because this would require simultaneous detection of the normal component of the desorbing molecules' translational energy over the entire forward hemisphere of solid angles. In contrast, both the angle-resolved and angle-integrated total translational energy distributions presented in Fig. 7 are measurable in the laboratory. Note that the total translational energy distributions are peaked away from the zero of energy, consistent with the passage of the desorbing molecules over an exit channel barrier. Unfortunately, heating low coverages of CH_{3(c)} and H_(c) on Pt(111) leads to CH_{3(c)} decomposition rather than hydrogenation. Methane product fluxes from associative desorption in the zero coverage limit are not experimentally available to test the PC-MURT detailed balance predictions. However, by coadsorbing relatively high cover-

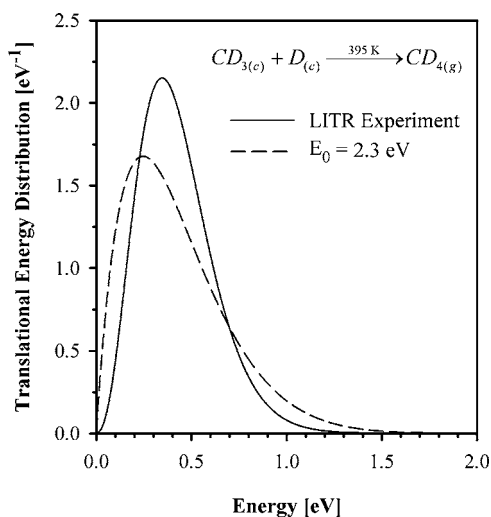


FIG. 13. Product translational energy distributions at the surface normal for the laser-induced thermal reaction (LITR) $CD_{3(c)} + D_{(c)} \rightarrow CD_{4(g)}$ on Pt(111) assumed to occur at the calculated peak surface temperature of 395 K (see Ref. 39). The PC-MURT prediction with $E_0 = 2.3$ eV for the product translational energy distribution is shown as the dashed curve. For both distributions the mean translational energy is 0.43 eV.

ages of $H_{(c)}$ the $CH_{3(c)}$ can be kinetically stabilized and the associative desorption of methane can be observed.³⁷

Although not explicitly compared here, the high coverage associative desorption experimental results of Ukraintsev and Harrison³⁷ and Watanabe *et al.*³⁹ are not consistent with the PC-MURT predictions for the reactive methane flux distributions for dissociative chemisorption on clean Pt(111) [cf. Figs. 7, 10, and 11 with 13–15]. This discrepancy is not

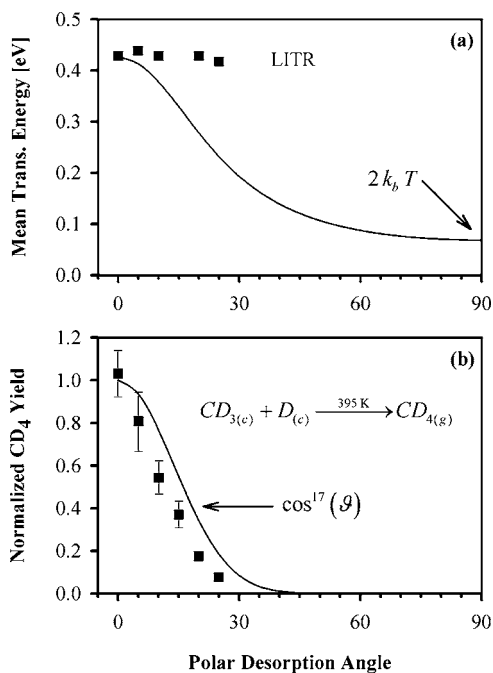


FIG. 14. Detailed balance predictions of (a) the variation of the product mean translational energy with desorption angle and (b) the product angular distribution for the LITR $CD_{3(c)} + D_{(c)} \rightarrow CD_{4(g)}$ on Pt(111) assumed to occur at the calculated peak surface temperature of 395 K. The solid squares are data from Watanabe *et al.* (Ref. 39) and the solid curves represent the PC-MURT predictions with $E_0 = 2.3$ eV.

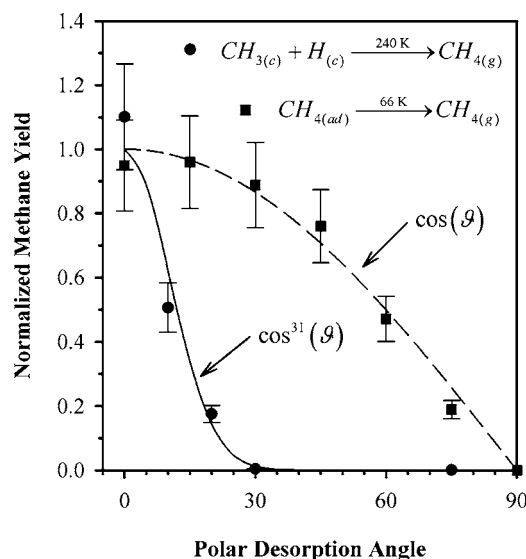


FIG. 15. Product angular distributions for the thermally induced methyl radical hydrogenation reaction (solid circles) on Pt(111) at 240 K surface temperature and the thermally induced molecular desorption of physisorbed methane (solid squares) (see Ref. 37). The detailed balance predictions of the PC-MURT are shown for $E_0 = 2.3$ eV as solid and dashed curves.

surprising because both the experiments of Ukraintsev and Harrison and Watanabe *et al.* were performed at close to saturation combined coverage of chemisorbed hydrogen and methyl radicals rather than in the zero coverage limit. Detailed balance needs only apply to the thermal fluxes of experiments performed under identical surface coverage and quasiequilibrium conditions. Arguing along Evans-Polanyi lines that as the surface coverage increases the methane dissociation products are destabilized and so too is the reactive transition state, increasing the CH_4 threshold energy for dissociation from its zero coverage value of $E_0 = 0.61 - 2.3$ eV recovers the mean translational energy of $\langle E_t \rangle = 0.43 \pm 0.01$ eV observed for the $\vartheta = 0^\circ$ CD_4 product from the high coverage laser-induced thermal reaction (LITR). The corresponding PC-MURT translational energy distribution is compared to the LITR distribution in Fig. 13.

Figure 14 compares the PC-MURT detailed balance predictions to the experimental results of Watanabe *et al.* for the angular variation of the mean translational energy and desorption yield for associatively desorbing CD_4 from Pt(111). The three-parameter PC-MURT simulations assume a high coverage value for the CH_4 reaction threshold energy of $E_0 = 2.3$ eV and retain the $\{\nu_D = 110 \text{ cm}^{-1}, s = 3\}$ CH_4 parameters derived from the studies of the $CH_4/Pt(111)$ initial dissociative sticking coefficients in the limit of zero coverage.²² Kinetic isotope effects²² shift these PC-MURT parameters to $\{E_0 = 2.345 \text{ eV}, \nu_D = 95 \text{ cm}^{-1}, s = 3\}$ for the $CD_4/Pt(111)$ system but we consistently label the high coverage parameter set by just its $CH_4/Pt(111)$ values. While the PC-MURT predicts a rather sharp drop in the mean translational energy as the desorption angle increases, the LITR experiments of Watanabe *et al.* show essentially no variation from 0° to 25° . According to Eqs. (41) and (53) and of the PC-MURT, at 90° from the surface normal the mean translational energy should fall to $2k_B T$.

Figure 15 shows the PC-MURT detailed balance predictions for the associative and molecular desorption of CH_4 from Pt(111) compared to the experimental results of Ukraintsev and Harrison. Regardless of the surface temperature, the PC-MURT predicts a $\cos \vartheta$ angular distribution for molecular desorption. In contrast, the PC-MURT predicts a temperature dependent angular distribution for associative desorption that broadens as the temperature increases. At the 240 K surface temperature of the CH_4 experiments of Ukraintsev and Harrison the PC-MURT predicts a $\cos^{31} \vartheta$ angular distribution for associative desorption, in good agreement with the experimentally observed $\cos^{37} \vartheta$ distribution. The PC-MURT distribution broadens to $\cos^{17} \vartheta$ at the 395 K surface temperature of the CD_4 experiments of Watanabe *et al.*

VI. DISCUSSION

In this section we return to more critically evaluate the practical applicability of the principle of detailed balance at equilibrium to the results of thermal associative desorption experiments for the methane/Pt(111) system. Although detailed balance has been successfully applied to the dissociative chemisorption and associative desorption of H_2 on multiple metal surfaces,³⁶ for gases that produce polyatomic chemisorbed species the possibility of secondary decomposition pathways is a complicating feature. Here, the principal question is whether the $\text{CH}_{3(c)} + \text{H}_{(c)} \rightleftharpoons \text{CH}_{4(g)}$ thermal equilibrium can be experimentally approximated amongst the surface species in the presence of competitive $\text{CH}_{3(c)}$ decomposition [i.e., can chemisorbed methyl be sufficiently kinetically stabilized against decomposition by coadsorbed $\text{H}_{(c)}$]. Although some authors have investigated the chemistry of methyl radicals on Pt(111),^{54,55} detailed kinetic information concerning chemisorbed methyl radical chemistry is generally lacking. If methyl decomposition is appreciable, then application of detailed balance, at least in the simple form presented above in Secs. IV and V, cannot be *rigorously* used to relate the results of associative desorption experiments to CH_4 dissociative chemisorption experiments or theoretical predictions. To illustrate this point, consider a hypothetical scenario in which 25% of the nascent $\text{CH}_{3(c)}$ formed by thermal $\text{CH}_{4(g)}$ dissociative chemisorption decomposes to $\text{CH}_{2(c)} + \text{H}_{(c)}$ while the other 75% of the nascent $\text{CH}_{3(c)}$ is hydrogenated. It may be that the energy distribution of the nascent $\text{CH}_{3(c)}$ that successfully decomposes is quite different from that for all the nascent $\text{CH}_{3(c)}$ formed. In true thermal equilibrium, the 25% loss of the nascent $\text{CH}_{3(c)}$ would be precisely compensated for by $\text{CH}_{2(c)}$ hydrogenation to replenish the nascent $\text{CH}_{3(c)}$, such that the $\text{CH}_{3(c)} + \text{H}_{(c)} \rightleftharpoons \text{CH}_{4(g)}$ equilibrium is dynamically sustained. In thermal associative desorption experiments, if the quasiequilibrium of chemisorbed surface species does not react similarly to compensate for the 25% decomposition channel of the “nascent” $\text{CH}_{3(c)}$ coverage then the resulting $\text{CH}_{4(g)}$ product flux may lack as much as 25% of the trajectories that a true equilibrium product distribution should contain. A final complication is that associative desorption experiments typically

desorb all the initially deposited reactants and hence the product results are integrated over a range of reactant surface coverages.

Indeed, for detailed balance at equilibrium to apply to the methane/Pt(111) system, in the strictest sense, requires identical experimental conditions and this applies equally to the coverage of chemisorbed species as well as to the pressure of gas above the surface. In practice we measure associative desorption distributions under UHV conditions that are far from equilibrium and the absence of a thermal gas above the surface that might drive collisionally induced desorption, etc., and thereby reduce the chemisorbed coverage under equilibrium conditions may be a concern.³⁶ For the methane/Pt(111) system we expect energy transfer to be dominated by the surface and not the gas above the surface because for reasonable energy transfer parameters the pressure of methane gas above the surface would have to be 600 bars at 800 K to generate the same collision rate between PCs and the ambient gas as is experienced between the PCs and the underlying surface. The effects of surface coverage,⁵⁶ however, cannot be argued away so simply and in the absence of experiments on the coverage dependence of the dissociative sticking coefficient we have simply assumed that the barrier is coverage dependent. This does not seem unreasonable because coverage dependent barriers have been observed for multiple systems including the dissociative chemisorption of N_2 on Ru(0001).⁴¹

In contrast to activated systems that show coverage dependent barriers to dissociative chemisorption, Mortensen *et al.*²⁹ have reported that the adiabatic barrier to dissociation of CH_4 on Ru(0001) is nearly independent of surface hydrogen coverage between 0 and 0.26 ML. Thus, it is perhaps instructive to compare and contrast the methane/Pt(111) and methane/Ru(0001) dissociative chemisorption systems. The first difference to note between these systems is that thermal programmed reaction of chemisorbed methyl and hydrogen on Pt(111) (Ref. 57) produces $\text{CH}_{4(g)}$ while on Ru(0001) (Ref. 29) the methyl undergoes decomposition and no observable $\text{CH}_{4(g)}$ is produced. These results indicate that the barrier to decomposition of chemisorbed methyl is more comparable to that for association with chemisorbed hydrogen on Pt(111) than on Ru(0001). Indeed, electronic structure theory computations on Pt(111) (Refs. 58–60) and Ru(0001) (Ref. 61) support this conclusion. On Pt(111) these barriers are predicted to be approximately equal and on Ru(0001) the barrier to associative desorption is predicted to be approximately twice that for methyl decomposition. Following our statistical premise and given the disparity of these reaction barriers on Ru(0001), we expect the number of open methyl decomposition channels to be huge even at the threshold for associative desorption, leading to little distortion of the exit channel distributions for desorbing CH_4 . On Pt(111), however, these barriers are quite comparable such that channels to decomposition and association are opening up at the same energies, leading to greater distortion of the observed CH_4 exit channel distributions. This argument seems plausible, given that associative desorption is excited thermally and thus the product distributions are strongly weighted towards low energy channels. However, whether or not detailed

balance is applicable to the methane/Pt(111) system remains an open question that can only be answered by experiment. Perhaps Laidler⁶² has put it best, warning that *wrong* conclusions are often drawn from the principles (of detailed balance) by applying them to systems that are not elementary and are not at equilibrium. As attractive as the principle of detailed balance may be, caution is warranted when applying it to new systems.

To conclude we note that Wei and Iglesia⁶³ have recently experimentally determined the activation energy for the dissociation of CH₄ on 1.6-wt % Pt/ZrO₂ at 873 K and 1 bar pressure to be 0.81 eV in close agreement with our CH₄/Pt(111) prediction [see Fig. 14(a) of Ref. 22] of $E_a = 0.69$ eV at the same temperature. In addition, Wei and Iglesia determined the kinetic isotope effect to be 1.58 at 873 K, again in close agreement with our CH₄/Pt(111) prediction of 2.5 [see Fig. 14(b) of Ref. 22]. It is encouraging that the simple PC-MURT model of dissociative chemisorption, informed by nonequilibrium molecular beam experiments on Pt(111), is able to provide reasonable predictions for some aspects of the thermal equilibrium sticking observed for supported Pt metal nanocrystallite catalysts that likely expose Pt(111) facets over only a portion of their surface. Surprisingly, the thermal dissociative sticking coefficient derived from the CH₄ turnover rate⁶³ for exposed surface atoms on the supported Pt catalysts at 873 K is roughly four orders of magnitude *lower* than the $S(873\text{ K}) = 1.5 \times 10^{-3}$ thermal dissociative sticking coefficient predicted by the PC-MURT for CH₄ on clean Pt(111).²² Similar differences between the CH₄ turnover rates on supported nanocrystallite metal catalysts and dissociative sticking coefficients on low index single crystals have been observed for Ni^{64,65,14} and Ir.^{66,67,27} These differences between the ability of the exposed atoms on metal nanocatalysts to turnover through a catalytic cycle involving CH₄ dissociative chemisorption and for atoms on low index single crystals to execute a single CH₄ dissociative chemisorption are intriguing and suggest that significant gains in the performance of methane reforming catalysts may still be achievable through improved catalyst processing and formulation.

VII. SUMMARY

The thermal activated dissociative chemisorption of methane on Pt(111) was investigated using a microcanonical unimolecular rate theory (MURT) model of gas-surface reactivity. The infinite frequency strong collision (IFSC), surface ergodic collision theory (SECT), and “Lenzer” density weighted exponential down energy transfer models for coupling a local hot spot to the surrounding substrate were developed and evaluated within the context of a master equation (ME)-MURT. The three-parameter physisorbed complex (PC)-MURT was shown to closely approximate the thermal sticking under any realistic energy transfer model. The IFSC ME-MURT and PC-MURT limits were shown to define outer bounds on the thermal dissociative sticking coefficient based on their limiting energy transfer behavior. Assuming an apparent threshold energy for CH₄ dissociative chemisorption of $E_0 = 0.61$ eV on clean Pt(111), the PC-MURT was used to

predict angle-resolved yield, translational, vibrational, and rotational distributions for the reactive methane flux at thermal equilibrium at 500 K. Given that methyl radical hydrogenation can only be experimentally observed when the CH₃ radicals are kinetically stabilized against decomposition by coadsorbed H, the PC-MURT was used to evaluate E_0 in the high coverage limit. A high coverage value of $E_0 = 2.3$ eV sufficed to reproduce the experimentally observed methane angular and translational energy distributions from thermal hydrogenation of methyl radicals. Although rigorous application of detailed balance arguments to the CH₄/Pt(111) reactive system cannot be made because thermal decomposition of the methyl radicals competes with hydrogenation, its approximate applicability would argue for a strong coverage dependence of E_0 with H coverage—a dependence not seen for methyl radical hydrogenation on Ru(0001) (Ref. 29), but not yet experimentally explored on Pt(111).

ACKNOWLEDGMENTS

This research was supported by the National Science Foundation (NSF) Grant No. 0415540 and by the donors of the American Chemical Society Petroleum Research Fund. Two of the authors (A.B. and H.L.A.) gratefully acknowledge fellowship support under NSF IGERT Grant No. 9972790. We thank Kurt K. Kolasinski for helpful discussions.

- ¹ K. Honkala, A. Hellman, I. N. Remediakis, A. Logadottir, A. Carlsson, S. Dahl, C. H. Christensen, and J. K. Nørskov, *Science* **307**, 555 (2005).
- ² H. Rauscher, *Surf. Sci. Rep.* **42**, 207 (2001).
- ³ J. F. Weaver, A. F. Carlsson, and R. J. Madix, *Surf. Sci. Rep.* **50**, 107 (2003).
- ⁴ L. B. F. Juurlink, P. R. McCabe, R. R. Smith, C. L. DiCologero, and A. L. Utz, *Phys. Rev. Lett.* **83**, 868 (1999).
- ⁵ R. C. Egeberg, S. Ullmann, I. Alstrup, C. B. Mullins, and I. Chorkendorff, *Surf. Sci.* **497**, 183 (2002).
- ⁶ M. B. Lee, Q. Y. Yang, S. L. Tang, and S. T. Ceyer, *J. Chem. Phys.* **85**, 1693 (1986).
- ⁷ P. M. Holmblad, J. Wambach, and I. Chorkendorff, *J. Chem. Phys.* **102**, 8255 (1995).
- ⁸ M. N. Carré and B. Jackson, *J. Chem. Phys.* **108**, 3722 (1998).
- ⁹ R. Milot and A. P. J. Jansen, *Phys. Rev. B* **61**, 15657 (2000).
- ¹⁰ L. Halonen, S. L. Bernasek, and D. J. Nesbitt, *J. Chem. Phys.* **115**, 5611 (2001).
- ¹¹ M. P. Schmid, P. Maroni, R. D. Beck, and T. R. Rizzo, *J. Chem. Phys.* **117**, 8603 (2002).
- ¹² R. D. Beck, P. Maroni, D. C. Papageorgopoulos, T. T. Dang, M. P. Schmid, and T. R. Rizzo, *Science* **302**, 98 (2003).
- ¹³ Y. Xiang and J. Z. H. Zhang, *J. Chem. Phys.* **118**, 8954 (2003).
- ¹⁴ H. L. Abbott, A. Bukoski, and I. Harrison, *J. Chem. Phys.* **121**, 3792 (2004).
- ¹⁵ R. R. Smith, D. R. Killelea, D. F. DelSesto, and A. L. Utz, *Science* **304**, 992 (2004).
- ¹⁶ A. Hirsimäki, S. Paavilainen, J. A. Nieminen, and M. Valden, *Surf. Sci.* **482**, 171 (2001).
- ¹⁷ G. R. Schoofs, C. R. Arumainayagam, M. C. McMaster, and R. J. Madix, *Surf. Sci.* **215**, 1 (1989).
- ¹⁸ A. C. Luntz and D. S. Bethune, *J. Chem. Phys.* **90**, 1274 (1989).
- ¹⁹ J. Harris, J. Simon, A. C. Luntz, C. B. Mullins, and C. T. Rettner, *Phys. Rev. Lett.* **67**, 652 (1991).
- ²⁰ A. V. Walker and D. A. King, *Phys. Rev. Lett.* **82**, 5156 (1999).
- ²¹ J. Higgins, A. Conjusteau, G. Scoles, and S. L. Bernasek, *J. Chem. Phys.* **114**, 5277 (2001).
- ²² A. Bukoski, D. Blumling, and I. Harrison, *J. Chem. Phys.* **118**, 843 (2003).
- ²³ T. Kondo, T. Sasaki, and S. Yamamoto, *J. Chem. Phys.* **118**, 760 (2003).

- ²⁴A. T. Gee, B. E. Hayden, C. Mormiche, A. W. Kleyn, and B. Riedmuller, *J. Chem. Phys.* **118**, 3334 (2003).
- ²⁵D. C. Seets, C. T. Reeves, B. A. Ferguson, M. C. Wheeler, and C. B. Mullins, *J. Chem. Phys.* **107**, 10229 (1997).
- ²⁶D. C. Seets, M. C. Wheeler, and C. B. Mullins, *J. Chem. Phys.* **107**, 3986 (1997).
- ²⁷H. L. Abbott and I. Harrison, *J. Phys. Chem. B* **109**, 10371 (2005).
- ²⁸J. H. Larsen, P. M. Holmblad, and I. Chorkendorff, *J. Chem. Phys.* **110**, 2637 (1999).
- ²⁹H. Mortensen, L. Diekhoner, A. Baurichter, and A. C. Luntz, *J. Chem. Phys.* **116**, 5781 (2002).
- ³⁰C. T. Rettner, H. E. Pfnur, and D. J. Auerbach, *Phys. Rev. Lett.* **54**, 2716 (1985).
- ³¹C. T. Rettner, H. E. Pfnur, and D. J. Auerbach, *J. Chem. Phys.* **84**, 4163 (1986).
- ³²A. Bukoski and I. Harrison, *J. Chem. Phys.* **118**, 9762 (2003).
- ³³H. L. Abbott, A. Bukoski, D. F. Kavulak, and I. Harrison, *J. Chem. Phys.* **119**, 6407 (2003).
- ³⁴O. Swang, K. Faegri, O. Gropen, U. Wahlgren, and P. Siegbahn, *Chem. Phys.* **156**, 379 (1991).
- ³⁵D. F. Kavulak, H. L. Abbott, and I. Harrison, *J. Phys. Chem. B* **109**, 685 (2005).
- ³⁶A. Hodgson, *Prog. Surf. Sci.* **63**, 1 (2000).
- ³⁷V. A. Ukraintsev and I. Harrison, *Surf. Sci.* **286**, L571 (1993).
- ³⁸V. A. Ukraintsev and I. Harrison, *J. Chem. Phys.* **101**, 1564 (1994).
- ³⁹K. Watanabe, M. C. Lin, Y. A. Gruzdov, and Y. Matsumoto, *J. Chem. Phys.* **104**, 5974 (1996).
- ⁴⁰I. Harrison, *Acc. Chem. Res.* **31**, 631 (1998).
- ⁴¹L. Diekhoner, H. Mortensen, A. Baurichter, and A. C. Luntz, *J. Chem. Phys.* **115**, 3356 (2001).
- ⁴²A. C. Luntz, *J. Chem. Phys.* **113**, 6901 (2000).
- ⁴³T. Baer and W. L. Hase, *Unimolecular Reaction Dynamics* (Oxford University Press, New York, NY, 1996).
- ⁴⁴J. R. Barker, L. M. Yoder, and K. D. King, *J. Phys. Chem. A* **105**, 796 (2001).
- ⁴⁵I. Oref and D. C. Tardy, *Chem. Rev. (Washington, D.C.)* **90**, 1407 (1990).
- ⁴⁶W. Forst, *Unimolecular Reactions: A Concise Introduction* (Cambridge University Press, Cambridge, UK, 2003).
- ⁴⁷W. H. Weinberg, in *Dynamics of Gas-Surface Interactions*, edited by C. T. Rettner and M. N. R. Ashfold (The Royal Society of Chemistry, Cambridge, 1991).
- ⁴⁸C. T. Reeves, D. C. Seets, and C. B. Mullins, *J. Mol. Catal. A: Chem.* **167**, 207 (2001).
- ⁴⁹S. Nordholm, B. C. Freasier, and D. L. Jolly, *Chem. Phys.* **25**, 433 (1977).
- ⁵⁰D. Nilsson and S. Nordholm, *J. Chem. Phys.* **116**, 7040 (2002).
- ⁵¹D. Nilsson and S. Nordholm, *J. Chem. Phys.* **119**, 11212 (2003).
- ⁵²T. Lenzer, K. Luther, K. Reihls, and A. C. Symonds, *J. Chem. Phys.* **112**, 4090 (2000).
- ⁵³G. Comsa and R. David, *Surf. Sci. Rep.* **5**, 145 (1985).
- ⁵⁴D. H. Fairbrother, X. D. Peng, M. Trenary, and P. C. Stair, *J. Chem. Soc., Faraday Trans.* **91**, 3619 (1995).
- ⁵⁵M. A. Petersen, S. J. Jenkins, and D. A. King, *J. Phys. Chem. B* **108**, 5909 (2004).
- ⁵⁶F. Zaera, *Acc. Chem. Res.* **35**, 129 (2002).
- ⁵⁷F. Zaera, *Surf. Sci.* **262**, 335 (1992).
- ⁵⁸C. T. Au, C. F. Ng, and M. S. Liao, *J. Catal.* **185**, 12 (1999).
- ⁵⁹A. Michaelides and P. Hu, *J. Am. Chem. Soc.* **122**, 9866 (2000).
- ⁶⁰A. Michaelides and P. Hu, *J. Chem. Phys.* **114**, 2523 (2001).
- ⁶¹I. M. Ciobica, F. Frechard, R. A. van Santen, A. W. Kleyn, and J. Hafner, *J. Phys. Chem. B* **104**, 3364 (2000).
- ⁶²K. J. Laidler, *Chemical Kinetics*, 3rd ed. (Harper and Row, New York, 1987).
- ⁶³J. M. Wei and E. Iglesia, *J. Phys. Chem. B* **108**, 4094 (2004).
- ⁶⁴J. M. Wei and E. Iglesia, *J. Catal.* **224**, 370 (2004).
- ⁶⁵B. O. Nielsen, A. C. Luntz, P. M. Holmblad, and I. Chorkendorff, *Catal. Lett.* **32**, 15 (1995).
- ⁶⁶J. M. Wei and E. Iglesia, *Angew. Chem., Int. Ed.* **43**, 3685 (2004).
- ⁶⁷J. M. Wei and E. Iglesia, *Phys. Chem. Chem. Phys.* **6**, 3754 (2004).